

COVER PAGE

Document downloaded by @DAEL

Mon Nov 23 04:30:22 2026
For personal use

When automatic English translation is provided, only the original document is authentic.
The EAA cannot be held responsible of any translation error

Bibliographical reference

Enhancing Sound Attenuation in Permeable Heterogeneous Materials via Diffusion Processes, Rodolfo Venegas and Claude Boutin, Acta Acustica **vol. 104** (Number 4), 2018, pp. 623-635

DOI
https://doi.org/10.3813/AAA.919202

Acta Acustica united with Acustica
Vol. 104 (2018) 623 – 635

DOI 10.3813/AAA.919202

Enhancing Sound Attenuation in Permeable Heterogeneous Materials via Diffusion Processes

Rodolfo Venegas[1,2], Claude Boutin[3]

[1] University of Salford, Acoustics Research Centre, M5 4WT Salford, United Kingdom.

[2] Univ. Austral of Chile, Institute of Acoustics, P.O. Box 567, Valdivia, Chile. rodolfo.venegas@uach.cl

[3] Université de Lyon – ENTPE, LGCB / LTDS UMR CNRS 5513, Rue Maurice Audin, 69518 Vaulx-en-Velin, France

Summary

This paper illustrates the concept of inducing multiple local non-equilibrium pressure states in permeable rigid-frame materials by means of introducing specific geometrical patterns or material heterogeneities locally. This results in enhanced sound attenuation that is mostly determined by the local non-equilibrium pressure states of diffusive type. We illustrate the results by introducing analytical models for the long-wavelength acoustical properties of i) a perforated porous matrix with concentric annular and cylindrical porous inclusions co-axially inserted in the perforations, and ii) a heterogeneous array of highly resistive porous cylinders. The models predictions are compared with numerical simulations showing good agreement.

PACS no. 4320.Bi,43.20Hq, 43.55.Ev

1. Introduction

Sound energy dissipation in rigid-frame gas-saturated porous materials is caused by viscosity and heat conduction effects [1, 2, 3]. Viscous dissipation is caused by a local production of thermal energy through the generation of viscous stresses, while the dissipation associated with heat conduction by heat exchanges between the fluid and the solid frame of the material. Conventional porous materials are quite efficient at attenuating sound at high frequencies. However, these do not usually perform well at attenuating low frequency sound [4]. In recent years, research on different directions has been undertaken to overcome this issue. Examples include investigations on sound propagation in permeable materials with inner resonating units [5, 6, 7, 8, 9, 10] (often referred to as "metamaterials"), graded-index porous materials [11], materials with dead-end pores [12], porous materials with multiple scales [13, 14, 15, 16, 17, 18, 19, 20, 21, 22], and porous composites [23, 24].

Of direct relevance to this work, let us mention that sound attenuation in double porosity materials with highly contrasted permeabilities [13, 14] is significantly determined by a single local non-equilibrium pressure state of diffusive type. This phenomenon, also known as pressure diffusion, is responsible for the unconventional acoustic behaviour of the material and, in particular, modifies the macroscopic mass balance. Such a modification leads to an increase of sound attenuation in a wide frequency band centred at the characteristic frequency associated with the pressure diffusion phenomenon.

Recently, a theory of acoustics of gas-saturated permeable heterogeneous materials with multiple local non-equilibrium pressure states has been developed and validated experimentally [22]. These materials, which are characterised by a highly permeable pore fluid network and much less permeable local heterogeneities, also display unconventional macroscopic acoustic behaviour.

This work makes use of the theory developed in [22] and illustrates the concept of inducing multiple local non-equilibrium pressure states in permeable materials by means of introducing specific geometrical patterns or material heterogeneities locally; being the aim the enhancement of sound attenuation. The introduction of the said patterns leads to geometrically-induced local heterogeneities that we will refer to as local geometrical heterogeneities.

Analytical models for the long-wavelength acoustical properties of i) a perforated porous matrix with concentric annular and cylindrical porous inclusions co-axially inserted in the perforations (see Figure 2), and ii) a heterogeneous array of highly resistive porous cylinders (see Figure 5) are introduced. It will be shown that the enhanced sound attenuation in these materials is determined by the local non-equilibrium pressure states, or, in other words, by pressure diffusion. The contribution to sound energy dissipation of pressure diffusion will be shown to be stronger than that traditionally associated with viscosity and thermal exchanges in conventional porous media. Note, however, that the physical origin of the losses caused by pressure diffusion is es sentially visco-thermal.

Received 19 June 2017,
accepted 12 May 2018.

© S. Hirzel Verlag · EAA

Document downloaded by @DAEL, 2026-11-23 04:30:24 - personal use only

The paper is organised as follows. The macroscopic equations that describe sound propagation in permeable heterogeneous materials that can support multiple local non-equilibrium pressure states [22] are derived in Section 2. Analytical models for the acoustical properties of the materials mentioned above are introduced in Sections 3 and 4, where we also provide examples to illustrate their properties and compare the models predictions with those obtained from numerical simulations. The main findings are summarised in the conclusions.

2. Theory

2.1. Geometry and main assumptions

Consider a periodic rigid-frame permeable heterogeneous material saturated with a Newtonian fluid. Figure 1 shows a diagram of the scales of the material and the relevant geometrical descriptors. The macroscopic characteristic length L is related to the sound wavelength λ through $L = \lambda/2\pi$ and largely exceeds all other characteristic lengths of the material.

The representative elementary volume (REV) of the material is denoted as Ω. This comprises the volume of the pore fluid network Ω_p and the volume of the local heterogeneities Ω_i, where the subscript $i = 1, \ldots, N$ is used to index the local heterogeneities, unless otherwise stated.

The size of the period of the material (or characteristic pore size) is represented by ℓ, while the characteristic sizes associated with the pores of the substrate materials constituting the local heterogeneities are denoted as l_i. These characteristic sizes satisfy $l_i \ll \ell$. Because of the large separation of scales, the local heterogeneities Ω_i are modelled as equivalent Darcy media. The volume fraction occupied by the pore fluid network (or mesoporosity) is $\phi_p = \Omega_p/\Omega$, while the volume fractions occupied by the local heterogeneities are $\varphi_i = \Omega_i/\Omega$. Hence one has that $\phi_p + \sum_i \varphi_i = 1$ and the total porosity of the material is $\Phi = \phi_p + \sum_i \varphi_i \phi_i$, where ϕ_i are the porosities of the local heterogeneities. Furthermore, the disparity in length scales between the macroscopic characteristic length and the size of the period of the material provides a small parameter $\varepsilon = \ell/L \ll 1$.

2.2. Local description

The equations of motion of the pore saturating fluid are the linearised equations of conservation of momentum (1), mass (2), and energy (3); and the equation of state (4). Note that harmonic dependence of the type $e^{j\omega t}$ is assumed and, because of linearity, this term is omitted throughout the paper.

$$\operatorname{div}(2\eta\overline{\mathbf{D}}(\mathbf{u}_p)) - \nabla p_p = j\omega\rho_0\mathbf{u}_p \quad \text{in} \quad \Omega_p, \tag{1}$$

$$j\omega\rho_p + \rho_0\nabla\cdot\mathbf{u}_p = 0 \quad \text{in} \quad \Omega_p, \tag{2}$$

$$\kappa\nabla\cdot\nabla\tau_p = j\omega\rho_0 c_p\tau_p - j\omega p_p \quad \text{in} \quad \Omega_p, \tag{3}$$

$$\frac{p_p}{P_0} = \frac{\rho_p}{\rho_0} + \frac{\tau_p}{T_0} \quad \text{in} \quad \Omega_p. \tag{4}$$

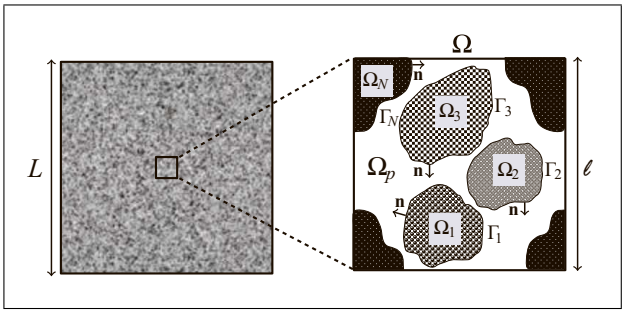

Figure 1. Diagram of the scales of a permeable heterogeneous material featuring a representative elementary volume (REV) Ω that comprises a pore fluid network Ω_p and local heterogeneities Ω_i with $i = 1, \ldots, N$.

Here η is the dynamic viscosity, κ is the thermal conductivity, and c_p is the specific heat capacity. p_p, ρ_p, τ_p, and $\mathbf{u}_p$ are the unknown complex-valued frequency-dependent fluid pressure, density, temperature, and velocity, respectively. The deviatoric strain rate tensor is given by $\overline{\mathbf{D}}(\mathbf{u}_p) = \frac{1}{2}\left(\nabla\mathbf{u}_p + (\nabla\mathbf{u}_p)^T\right) - \frac{1}{3}\nabla\cdot\mathbf{u}_p\mathbf{I}$, with $\mathbf{I}$ being the second-rank unitary tensor. Note that in Equation (1), we have neglected the bulk viscosity. The subscript 0 denotes equilibrium quantities, namely ρ_0 is the equilibrium density, and P_0 and T_0 are the ambient (equilibrium) pressure and temperature, respectively.

The local heterogeneities are modelled, due to the separation of scales $l_i/\ell \ll 1$, as equivalent Darcy media whose acoustic behaviour is governed by the following mass balance equations and fluid flow constitutive laws:

$$\nabla\cdot\mathbf{U}_i + j\omega p_i \mathsf{C}_i = 0 \ \text{ in } \ \Omega_i, \quad \mathbf{U}_i = -\frac{\mathbf{k}_i}{\eta}\cdot\nabla p_i, \tag{5}$$

where $\mathbf{U}_i$ and p_i are the Darcy velocities and pressures in the local heterogeneities, respectively. The effective parameters C_i and $\mathbf{k}_i$ are the known effective compressibilities and viscous permeabilities of the materials the local heterogeneities are made of. In general, these are complex valued and frequency dependent. For the particular case of local heterogeneities made of single porosity materials and taking into account a viscosity dominated flow in their micropores and a visco-inertial flow regime in the pores, the said effective parameters may be approximated by their static values, as detailed below. As in [13, 14, 22], their dependence in frequency will be considered since this will allow to identify a global characteristic frequency and obtain the correct limiting values of the effective parameters associated with the macroscopic description of sound propagation. Furthermore, if the local heterogeneities are made of materials experiencing inner dynamic states, e.g. double porosity [13, 14], multiscale sorptive [17, 18, 20, 21] or permeo-elastic [25] media, a strong dependence on frequency of the said effective parameters can be observed while fully respecting the separation of scales that permits the modelling of the local heterogeneities as enriched Darcy media.

The following boundary conditions on the pore-heterogeneities interfaces Γ_i representing the continuity of

Document downloaded by @DAEL, 2026-11-23 04:30:24 - personal use only

pressure and of temperature Equation (6) and the continuity of mass flux Equation (7) are considered (with $\mathbf{n}$ being the outward-pointing normal vector and τ_i being the mean temperature variations in the local heterogeneities),

$$p_p = p_i \quad \text{and} \quad \tau_p = \tau_i \quad \text{on} \quad \Gamma_i, \tag{6}$$

$$\rho_0 \mathbf{u}_p \cdot \mathbf{n} = \rho_0 \mathbf{U}_i \cdot \mathbf{n} \quad \text{on} \quad \Gamma_i. \tag{7}$$

In formulating the boundary conditions Equation (7), because of the assumed large separation of scales $l_i/\ell \ll 1$, i) the continuity of the tangential mass flux is not required, as tacitly considered in [22]; and ii) possible perturbation of the pore-scale fields due to boundary effects are neglected.

2.3. Physical analysis

This section provides an analysis of the physics of the local description presented in the previous section. This analysis will be used in the next section where the homogenisation procedure is described.

As in long-wavelength sound propagation in conventional porous media, it is considered, from a physical point of view, that [3]

i) the flow is driven by a macroscopic pressure gradient, and

ii) the fluid velocity and its rate of deviatoric deformation vary at the pore scale.

This respectively leads to the following estimates: $|\nabla p| = O(p_{pc}/L)$ and $|\mathrm{div}(2\eta\overline{\mathbf{D}}(\mathbf{u}_p))| = O(\eta_c u_{pc}/\ell^2)$. Here and in what follows the subscript c indicates a characteristic value of a given quantity. For example, u_{pc} is a characteristic value of $|\mathbf{u}_p|$.

We are interested in the case in which the viscous and inertial terms are balanced by the pressure gradient in the oscillatory Stokes equation (1) since it provides the richest flow regime. Hence, the three terms in Equation (1) are of the same order of magnitude, i.e.

$$O\Big(\frac{\eta_c u_{pc}}{\ell^2}\Big) = O\big(\omega_c \rho_{0c} u_{pc}\big) = O\Big(\frac{p_{pc}}{L}\Big). \tag{8}$$

Assuming that the divergence of the velocity varies according to the sound wavelength (or macroscopic size), one has that $|\nabla \cdot \mathbf{u}_p| = O(u_{pc}/L)$. Considering that this term is balanced out by the rate of volume variations in the equation of conservation of mass (2), one obtains that

$$O\Big(\frac{u_{pc}}{L}\Big) = O\Big(\frac{\omega_c \rho_c}{\rho_{0c}}\Big). \tag{9}$$

Regarding the equation of conservation of energy (3), since the temperature varies at the pore scale, one has that $|\kappa \nabla \cdot \nabla \tau_p| = O(\kappa_c \tau_{pc}/\ell^2)$. Furthermore, to capture the thermal effects in the pore fluid network, we consider that the estimations of the three terms in Equation (3) are of the same order of magnitude, i.e.

$$O\Big(\frac{\kappa_c \tau_{pc}}{\ell^2}\Big) = O\big(\omega_c \rho_{0c} c_{pc} \tau_{pc}\big) = O\big(\omega_c p_{pc}\big). \tag{10}$$

On the other hand, the three terms in the Equation of state (4) are of the same order of magnitude, namely

$$O\Big(\frac{p_{pc}}{P_{0c}}\Big) = O\Big(\frac{\tau_{pc}}{T_{0c}}\Big) = O\Big(\frac{\rho_{pc}}{\rho_{0c}}\Big). \tag{11}$$

The Darcy velocities and pressure in Equation (5) fluctuate at the pore scale. Hence the terms in these equations are estimated as $|\nabla \cdot \mathbf{U}_i| = O(U_{ic}/\ell)$ and $|\mathrm{j}\omega p_i \mathsf{C}_i| = O(\omega_c p_{ic} C_{ic})$, and $|-\mathbf{k}_i \cdot \nabla p_i/\eta| = O(k_{ic} p_{ic}/\eta_c \ell)$. Furthermore, we consider that the terms in the equations of conservation of mass (5)a are of the same order of magnitude, which is also the case for those involved in the fluid flow constitutive laws (5)b, i.e.

$$O\Big(\frac{U_{ic}}{\ell}\Big) = O\big(\omega_c p_{ic} C_{ic}\big), \quad O(U_{ic}) = O\Big(\frac{k_{ic} p_{ic}}{\eta_c \ell}\Big). \tag{12}$$

Due to continuity of pressure on the interfaces Γ_i [Equation (6)a], the pressures are of the same order of magnitude, i.e. $O(p_{pc}) = O(p_{ic})$. On the other hand, by making use of the continuity of heat fluxes one obtains [13] $O(\kappa_c \tau_{pc}/\ell) = O(\kappa_c \tau_{ic}/l_i)$. Hence the ratio between the characteristic values τ_{ic} and τ_{pc} is estimated as $\tau_{ic}/\tau_{pc} = O(\kappa_c l_i/\kappa_c \ell)$.

From Equation (8) one can assess the mass flux generated by the carrying wave in the pores as $\rho_{0c} u_{pc} = O(\rho_{0c} p_{pc} \ell^2/\eta_c L)$, while from Equation (12) the mass flux pulsed from the local heterogeneities as $\rho_{0c} U_{ic} = O(\rho_{0c} k_{ic} p_{ic}/\eta_c \ell)$. Using these estimates the mass flux ratio $\mathcal{U}_i = |\rho_0 \mathbf{U}_i \cdot \mathbf{n}|/|\rho_0 \mathbf{u}_p \cdot \mathbf{n}|$ is estimated as

$$\mathcal{U}_i = O\Big(\frac{U_{ic}}{u_{pc}}\Big) = O\Big(\frac{k_{ic} p_{ic}}{\eta_c \ell} \frac{\eta_c L}{p_{pc} \ell^2}\Big) = O\Big(\frac{k_{ic}}{\ell^2} \frac{L}{\ell}\Big). \tag{13}$$

This estimation reflects that the mass flux pulsed from the local heterogeneities is much smaller than that in the pores since $\mathcal{U}_i = O(\mathbb{U}_{ic} \ell/L) = O(\varepsilon)$ with $\mathbb{U}_{ic} = (\sqrt{k_{ic}} L/\ell^2)^2 = O((l_i L/\ell^2)^2) = O(1)$. In addition, this estimation largely determines the validity range of the upscaled model to be derived, which holds as long as ℓ and l_i are well separated, i.e. $l_i/\ell = O(\varepsilon)$.

2.4. Homogenisation procedure

This section makes use of the homogenisation methodology based on dimensional analysis introduced by Auriault [26, 3].

Let us use the two characteristic lengths ℓ and L and the physical space variable $\mathbf{X}$ to define two dimensionless variables, namely $\mathbf{x}^* = \mathbf{X}/L$ and $\mathbf{y}^* = \mathbf{X}/\ell$. These dimensionless variables respectively describe variations on the macroscopic and microscopic scales and, due to the large separation of scales, are assumed independent. As a consequence of the introduction of the two spatial variables, the large separation of scales, and periodicity, the unknown physical variables are, a priori, considered to be functions of $\mathbf{x}^*$ and $\mathbf{y}^*$ and are $\mathbf{y}^*$ – periodic.

Furthermore, considering once again the large scale separation and invoking the chain rule, the dimensionless gradient operator is given by $L\nabla_{\mathbf{X}} = \nabla_{\mathbf{x}^*} + \varepsilon^{-1}\nabla_{\mathbf{y}^*}$. To simplify the notation we will consider later that $\nabla_* = L\nabla_{\mathbf{X}}$.

Document downloaded by @DAEL, 2026-11-23 04:30:24 - personal use only

The local description Equations (1)–(7) is then written in dimensionless form. To do so we consider that the variables and parameters are normalised by characteristic values. For instance, the dimensionless fluid velocity is $\mathbf{u}_p^* = \mathbf{u}_p/u_{pc}$ and the dimensionless viscosity is $\eta^* = \eta/\eta_c$. As an example of the adimensionalization process, let us consider the oscillatory Stokes equation (1) and insert the dimensionless variables and parameters in it. For instance, the fluid velocity $\mathbf{u}_p$ in Equation (1) is replaced by $u_{pc}\mathbf{u}_p^*$, the dynamic viscosity by $\eta_c\eta^*$, etc. This yields

$$\mathcal{Q}_L \mathrm{div}_*\left(2\eta^*\overline{\mathbf{D}}_*(\mathbf{u}_p^*)\right) - \mathcal{P}_L\nabla_* p_p^* = \mathrm{j}\omega^*\rho_0^*\mathbf{u}_p^*, \qquad (14)$$

where $\mathcal{Q}_L = u_{pc}\eta_c/\omega_c\rho_{0c}u_{pc}L^2$ and $\mathcal{P}_L = p_c/\omega_c\rho_{0c}u_{pc}L$. Using Equation (8), $\mathcal{Q}_L$ is given by $\mathcal{Q}_L = \mathcal{Q}_c\ell^2/L^2 = \mathcal{Q}_c\varepsilon^2$ with $\mathcal{Q}_c = u_{pc}\eta_c/\omega_c\rho_{0c}u_{pc}\ell^2 = O(1)$. Similarly, $\mathcal{P}_L$ is given by $\mathcal{P}_L = \mathcal{P}_c$ with $\mathcal{P}_c = p_c/\omega_c\rho_{0c}u_{pc}L = O(1)$.

Hence the dimensionless equation of conservation of momentum becomes (with $\nabla_* = \nabla_{\mathbf{x}^*} + \varepsilon^{-1}\nabla_{\mathbf{y}^*}$)

$$\mathcal{Q}_c\varepsilon^2\mathrm{div}_*\left(2\eta^*\overline{\mathbf{D}}_*(\mathbf{u}_p^*)\right) - \mathcal{P}_c\nabla_* p_p^* = \mathrm{j}\omega^*\rho_0^*\mathbf{u}_p^*. \qquad (15)$$

Following the same procedure and keeping in mind the physical analysis [see Equations (9), (10) and (11)], one can obtain the following dimensionless equations of conservation of mass and energy

$$\mathrm{j}\omega^*\left(\frac{p_p^*}{P_0^*} - \frac{\tau_p^*}{T_0^*}\right) + \overbrace{\frac{u_{pc}/L}{\omega_c\rho_{pc}/\rho_{0c}}}^{S_c=O(1)}\nabla_*\cdot\mathbf{u}_p^* = 0, \qquad (16)$$

$$\underbrace{\frac{\kappa_c\tau_{pc}/\ell^2}{\omega_c\rho_{0c}c_{pc}\tau_{pc}}}_{\mathcal{N}_c=O(1)}\varepsilon^2\kappa^*\nabla_*^2\tau_p^* = \mathrm{j}\omega^*\rho_0^*c_p^*\tau_p^* - \mathrm{j}\omega^* p_p^*\underbrace{\frac{\omega_c p_{pc}}{\omega_c\rho_{0c}c_{pc}\tau_{pc}}}_{\mathbb{N}_c=O(1)}. \qquad (17)$$

The mass balance equations and fluid flow constitutive laws Equations (5) in dimensionless form are given by Equations (18) and (19). Note that in formulating these equations, we have made use of Equation (12).

$$\overbrace{\frac{U_{ic}}{\ell\omega_c p_{ic}C_{ic}}}^{\mathcal{M}_{ic}=O(1)}\varepsilon\nabla_*\cdot\mathbf{U}_i^* + \mathrm{j}\omega^* p_i^*\mathsf{C}_i^* = 0, \qquad (18)$$

$$\mathbf{U}_i^* = -\underbrace{\frac{k_{ic}p_{ic}}{\ell U_{ic}\eta_c}}_{\mathcal{W}_{ic}=O(1)}\varepsilon\frac{\mathbf{k}_i^*}{\eta^*}\cdot\nabla_* p_i^*, \qquad (19)$$

It is convenient to eliminate the Darcy velocities. By doing so, one obtains the following equations [with $\mathbb{D}_{ic} = \mathcal{M}_{ic}\mathcal{W}_{ic} = k_{ic}/\ell^2\omega_c C_{ic}\eta_c = O(1)$]

$$\mathbb{D}_{ic}\varepsilon^2\nabla_*\cdot\left(-\frac{\mathbf{k}_i^*}{\eta^*\mathsf{C}_i^*}\cdot\nabla_* p_i^*\right) + \mathrm{j}\omega^* p_i^* = 0. \qquad (20)$$

The boundary conditions Equations (6) and (7) stating the continuity of pressure, temperature, and mass flux in dimensionless form are given by [see also Equation (13) and the paragraph after Equation (12)]

$$p_p^* = \mathbb{P}_{ic}p_i^*, \quad \tau_p^* = \frac{\tau_{ic}}{\tau_{pc}}\tau_i^* \quad \text{i.e.} \quad \tau_p^* = \mathbb{T}_{ic}\varepsilon\tau_i^*; \qquad (21)$$

$$\rho_0^*\mathbf{u}_p^*\cdot\mathbf{n} = \rho_0^*\frac{U_{ic}}{u_{pc}}\mathbf{U}_i^*\cdot\mathbf{n} \quad \text{i.e.} \quad \mathbf{u}_p^*\cdot\mathbf{n} = \mathbb{U}_{ic}\varepsilon\mathbf{U}_i^*\cdot\mathbf{n}, \qquad (22)$$

where $\mathbb{P}_{ic} = p_{ic}/p_{pc} = O(1)$, $\mathbb{T}_{ic} = \kappa_c/\kappa_c = O(1)$, and $\mathbb{U}_{ic} = (\sqrt{k_{ic}}L/\ell^2)^2 = O(1)$.

In summary, the rescaled dimensionless local description is given by Equations (15)–(22). This set governs the motion of the pore saturating visco-thermal fluid, modelled as a linear compressible fluid, interacting with the local heterogeneities modelled as Darcy media. In particular, the fluid in the pore fluid network is compressible and interacts with the effective linear compressible fluid in the local heterogeneities. However, considering the local flow, the fluid saturating the pore fluid network behaves asymptotically as incompressible at the leading order. Nevertheless, at the macroscopic level, the fluid compressibility is taken into account.

The next step in the homogenisation process consists in looking for the variables in the form of asymptotic expansions in powers of the small parameter ε, e.g. $p_p^*(\mathbf{x}^*, \mathbf{y}^*) = \sum_{k=0}^{\infty}\varepsilon^k p_p^{*(k)}(\mathbf{x}^*, \mathbf{y}^*)$. These series are then replaced into Equations (15)–(22) and the terms of the same order are identified.

At ε^{-1}, it follows from the equation of conservation of momentum that $\nabla_{\mathbf{y}^*}p_p^{*(0)} = \mathbf{0}$, which means that the pressure $p_p^{*(0)} = p^{*(0)}(\mathbf{x}^*)$ is a macroscopic variable. Further identification provides the oscillatory Stokes and heat conduction problems leading to the dynamic Darcy's law and its thermal analogous (see e.g. [1, 2]). As detailed in the Appendix, the leading-order pressures $p_i^{*(0)}$ are governed by diffusion equations formulated in the local heterogeneities with the leading-order pore pressure $p^{*(0)}$ being imposed on the local heterogeneities-pore interfaces. The mathematical steps leading to the solution of these equations are also shown in the Appendix.

The effective equations governing sound propagation in the class of materials being investigated are then obtained as outlined in the next section.

Remark: The present methodology requires the direct and inverse passage from the dimensional space to the dimensionless space. This intricate process can be circumvented and the formulation is alleviated (see e.g. [5, 8, 20, 21, 25, 22]). This can be done cautiously at the cost of what might be perceived as an abuse of notation in the intermediate steps of the process where the dimensional and dimensionless variables are noted in the same manner.

Document downloaded by @DAEL, 2026-11-23 04:30:24 - personal use only

2.5. Macroscopic acoustic description

Applying the operator $\langle\cdot\rangle_* = \frac{1}{\Omega^*}\int_{\Omega_p^*}\cdot\mathrm{d}\Omega^*$ to the leading-order mass balance equation yields

$$\mathrm{j}\omega^*\left\langle\frac{p^{*(0)}}{P_0^*}-\frac{\tau_p^{*(0)}}{T_0^*}\right\rangle_* + \mathcal{S}_c\nabla_{\mathbf{x}^*}\cdot\langle\mathbf{u}_p^{*(0)}\rangle_* = -\mathcal{S}_c\langle\nabla_{\mathbf{y}^*}\cdot\mathbf{u}_p^{*(1)}\rangle_*. \tag{23}$$

The left-hand side terms correspond to those that appear in the macroscopic mass balance of a material with perfectly impervious local heterogeneities. The right-hand side term is a source term that accounts for the contribution of the local heterogeneities [22] to the macroscopic acoustic behaviour. This is calculated by

i) making successive use of the divergence theorem,

ii) noting that the resulting surface integrals on opposite boundaries of the cell cancel out due to periodicity, and

iii) using Equation (22) identified at ε^1 and Equation (18) at ε^0.

The final result is

$$\mathcal{S}_c\left\langle\nabla_{\mathbf{y}^*}\cdot\mathbf{u}_p^{*(1)}\right\rangle_* = \mathrm{j}\omega^*\sum_i^N\frac{\mathcal{S}_c\mathbb{U}_{ic}}{\mathcal{M}_{ic}\mathbb{P}_{ic}}\mathsf{C}_i^*\frac{1}{\Omega^*}\int_{\Omega_i^*}\mathbb{P}_{ic}p_i^{*(0)}\,\mathrm{d}\Omega^*,$$

where the integral involved is given by Equation (A8).

The final step in the homogenisation methodology being used corresponds to expressing the macroscopic description in physical dimensional form. An example of this procedure is provided at the end of the Appendix for the solution of the pressure diffusion problems (see also, for example, page 203 in [3] for the dynamic Darcy's law).

The macroscopic equations in physical dimensional form that describe sound propagation in permeable heterogeneous materials with multiple local non-equilibrium pressure states are the effective mass balance equation (24) and the dynamic Darcy's law Equation (25), namely [22]

$$\nabla_{\mathbf{X}}\cdot\left\langle\mathbf{u}_p^{(0)}\right\rangle + \mathrm{j}\omega p^{(0)}\mathsf{C}(\omega) = 0, \tag{24}$$

$$\left\langle\mathbf{u}_p^{(0)}\right\rangle = -\frac{\mathbf{k}(\omega)}{\eta}\cdot\nabla_{\mathbf{X}}p^{(0)}, \tag{25}$$

where $\left\langle\mathbf{u}_p^{(0)}\right\rangle$ is the dynamic Darcy velocity, $\Omega\langle\cdot\rangle = \int_{\Omega_p}\cdot\mathrm{d}\Omega$, and the dynamic viscous permeability $\mathbf{k}(\omega)$ and effective compressibility $\mathsf{C}(\omega)$ are given by

$$\mathbf{k}(\omega)\approx\mathbf{k}_p(\omega), \tag{26}$$

$$\mathsf{C}(\omega) = \mathsf{C}_p(\omega) + \sum_{i=1}^N\varphi_i\mathsf{C}_i(\omega)\mathcal{F}_i(\omega). \tag{27}$$

The dynamic viscous permeability $\mathbf{k}_p(\omega)$ is calculated as detailed in [1, 2, 29, 22], while the effective compressibility $\mathsf{C}_p(\omega)$ is given by

$$\mathsf{C}_p(\omega) = \frac{\phi_p}{P_0}\left(1-\frac{\gamma-1}{\gamma}\frac{\mathrm{j}\omega}{\omega_{tp}}\frac{\Theta_p(\omega)}{\Theta_{0p}}\right), \tag{28}$$

where γ is the adiabatic exponent, $\Theta_p(\omega)$ is the dynamic thermal permeability (see [2] for its definition and recipe for its calculation) and $\Theta_{0p} = \Theta_p(\omega = 0)$. The thermal characteristic frequency ω_{tp} determining the transition from isothermal to adiabatic sound propagation in the pore space is given by

$$\omega_{tp} = \frac{\phi_p\kappa}{\rho_0 c_p\Theta_{0p}}. \tag{29}$$

The effective compressibilities C_i can be calculated using Equation (28) with the subscript p being replaced by i. For example, ϕ_p becomes ϕ_i, $\Theta_p(\omega)\to\Theta_i(\omega)$, $\omega_{tp}\to\omega_{ti}$, etc. Note that these effective compressibilities may be approximated by their static value $\mathsf{C}_{0i} = \phi_i/P_0$ when the local heterogeneities are made of single porosity materials and $l_i/\ell\ll 1$.

The functions $\mathcal{F}_i(\omega)$ associated with the pressure diffusion functions $B_i(\omega)$, which are defined in Equation (A11), are given by

$$\mathcal{F}_i(\omega) = 1-\frac{\mathrm{j}\omega}{\omega_{bi}}\frac{B_i(\omega)}{B_{0i}}\frac{\mathcal{D}_{0i}}{\mathcal{D}_i(\omega)}, \tag{30}$$

where $B_{0i} = B_i(\omega = 0)$ and $\mathcal{D}_i(\omega)$ are the pressure diffusivities (see Equation A11). We recall that, for simplicity in the notation, the local heterogeneities have been considered as isotropic, i.e. $\mathbf{k}_i(\omega) = \mathcal{K}_i(\omega)\mathbf{I}$. Further noticing that the pressure diffusivities may be approximated by their static value $\mathcal{D}_{0i} = \mathcal{K}_{0i}/\eta\mathsf{C}_{0i}$, where $\mathcal{K}_{0i} = \mathcal{K}_i(\omega = 0)$, leads to $\mathcal{F}_i(\omega) = 1-\mathrm{j}\omega B_i(\omega)/B_{0i}\omega_{bi}$ with the pressure diffusion characteristic frequencies being given by

$$\omega_{bi} = \frac{\varphi_i\mathcal{D}_{0i}}{B_{0i}}. \tag{31}$$

The characteristic frequencies ω_{bi} and $\omega_{tz} = \phi_z\kappa/\rho_0 c_p\Theta_{0z}$, with the index $z = p$ for the highly permeable pore network and $z = i$ for the local heterogeneities, largely determine the behaviour of the effective compressibility since $\mathcal{F}_i(\omega\ll\omega_{bi}) = 1-j\omega/\omega_{bi}$, $\mathcal{F}_i(\omega\gg\omega_{bi}) = 0$, $P_0\mathsf{C}_z(\omega\ll\omega_{tz}) = \phi_z(1-(\gamma-1)\mathrm{j}\omega/\omega_{tz}\gamma)$, and $P_0\mathsf{C}_z(\omega\gg\omega_{tz}) = \phi_z/\gamma$. Hence, the effective compressibility takes the limiting values

$$P_0\mathsf{C}_{lf}(\omega) = \Phi-\frac{\mathrm{j}\omega}{\omega_c}\quad\text{and}\quad P_0\mathsf{C}_{hf} = \frac{\phi_p}{\gamma}, \tag{32}$$

where $\mathsf{C}_{lf}(\omega) = \mathsf{C}\left(\omega\ll\min(\omega_{tz},\omega_{bi})\right)$ and $\mathsf{C}_{hf} = \mathsf{C}\left(\omega_{ti}\gg\omega\gg\max(\omega_{tp},\omega_{bi})\right)$, and ω_c is a global characteristic frequency defined by

$$\frac{1}{\omega_c} = \frac{\gamma-1}{\gamma}\frac{\phi_p}{\omega_{tp}} + \sum_i\varphi_i\phi_i\left(\frac{\gamma-1}{\gamma}\frac{1}{\omega_{ti}}+\frac{1}{\omega_{bi}}\right). \tag{33}$$

Further assuming that the material is macroscopically isotropic, the dynamic viscous permeability becomes $\mathbf{k}_p(\omega) = \mathcal{K}_p(\omega)\mathbf{I}$. Then, the characteristic impedance

Document downloaded by @DAEL, 2026-11-23 04:30:24 - personal use only

$Z(\omega)$ and wave number $q(\omega)$ of the material are given by (with $\mathcal{K}(\omega) = \mathcal{K}_p(\omega)$)

$$Z(\omega) = \sqrt{\frac{\eta}{\mathrm{j}\omega\mathcal{K}(\omega)\mathsf{C}(\omega)}}, \quad q(\omega) = \omega\sqrt{\frac{\eta\mathsf{C}(\omega)}{\mathrm{j}\omega\mathcal{K}(\omega)}}. \tag{34}$$

Using these equations one can calculate the surface impedance $Z_w(\omega)$, pressure reflection coefficient $R(\omega)$, and sound absorption coefficient $\alpha(\omega)$ of a rigidly-backed layer of material of thickness d via

$$Z_w(\omega) = -\mathrm{j}Z(\omega)\cot(q(\omega)d), \tag{35}$$

$$R(\omega) = \frac{Z_w(\omega) - Z_0}{Z_w(\omega) + Z_0}, \tag{36}$$

$$\alpha(\omega) = 1 - |R(\omega)|^2,$$

where $Z_0 = \rho_0 c_0$ is the characteristic impedance of the fluid adjacent to the material and $c_0 = \sqrt{\gamma P_0/\rho_0}$ is its speed of sound.

In summary, the macroscopic acoustic description, given by Equations (24) and (25), allows us to conclude that, at the leading order, the dynamic Darcy's law and its associated effective parameter, i.e. the dynamic viscous permeability, are not modified by the physical processes occurring in the local heterogeneities. Conversely, the effective compressibility becomes modified by the multiple local non-equilibrium pressure states. Such a modification translates into an enhanced sound attenuation around the pressure diffusion characteristic frequencies ω_{bi}. These can be tuned to increase the frequency band where sound attenuation in permeable heterogeneous materials is higher, as it will be shown in the next sections.

As a remark, let us mention that similarly to the case of double porosity poroelastic media with highly contrasted permeabilities [19], including the frame elasticity of the local heterogeneities into the modelling will lead to a Biot-type macroscopic description in which the effective stiffness and coupling tensors as well as the compressibility are affected by the multiple local non-equilibrium pressure states. A detailed investigation of the said type of media may be an extension of this work.

3. Material with local geometrical heterogeneities

This section exemplifies the concept of inducing multiple local non-equilibrium pressure states in permeable heterogeneous materials by means of introducing local geometrical heterogeneities. The aim is to provide a practically useful way of transforming a highly resistive porous material into an efficient porous sound absorber. To illustrate the concept, we introduce an analytical model for the acoustical properties of a perforated porous matrix with concentric annular and cylindrical porous inclusions inserted in the perforations and provide examples of its acoustical properties. For simplicity, we will refer to this material as heterogeneous sound absorber.

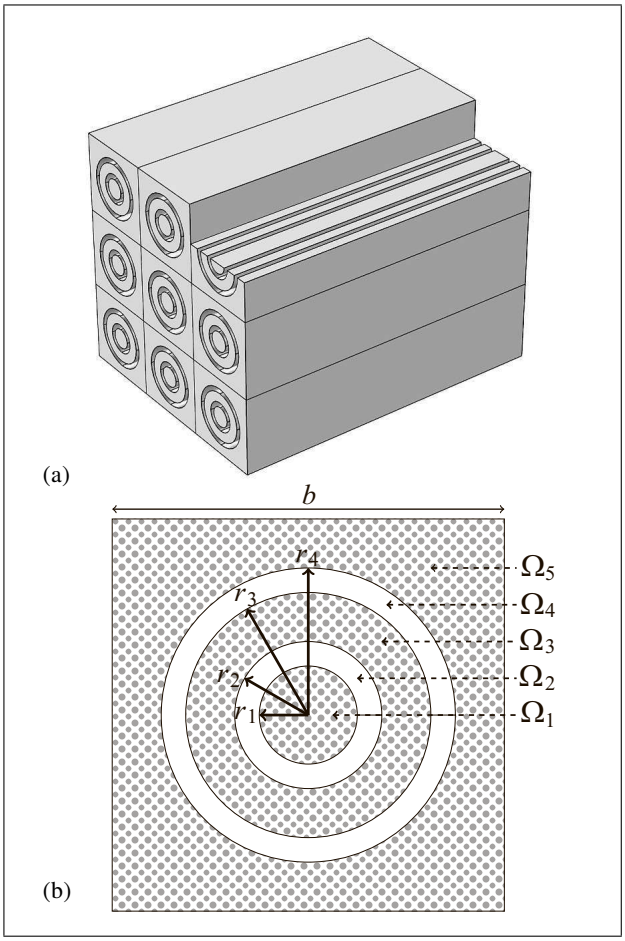

Figure 2. Geometry (a) and elementary cell (b) of a perforated porous matrix Ω_5 with concentric porous annular Ω_3 and cylindrical Ω_1 inclusions co-axially inserted in the perforations. The pore fluid network comprises two annular pores Ω_2 and Ω_4 per elementary cell.

3.1. Analytical model

The geometry and elementary cell of the heterogeneous sound absorber are shown in Figure 2. The elementary cell features local heterogeneities Ω_1, Ω_3, and Ω_4; and a pore fluid network determined by the annular pores Ω_2 and Ω_4.

The local heterogeneity Ω_1 is a cylindrical porous inclusion with radius r_1 and volume fraction $\varphi_1 = \pi r_1^2/b^2$, where b is the cell size. The local heterogeneity Ω_3 is an annular porous inclusion with inner and outer radii r_2 and r_3, radii ratio $\mathcal{R}_3 = r_2/r_3$, and volume fraction $\varphi_3 = \pi r_3^2(1 - \mathcal{R}_3^2)/b^2$. The porous matrix Ω_5 is characterised by r_4 and $\varphi_5 = 1 - \pi r_4^2/b^2$. The porous matrix and inclusions are made out of the same granular material having a grain radius r_g and porosity ϕ_g.

The annular pore Ω_2 (resp. Ω_4) is characterised by its inner and outer radii r_1 and r_2 (resp. r_3 and r_4), the radii ratio $\mathcal{R}_2 = r_1/r_2$ (resp. $\mathcal{R}_4 = r_3/r_4$) and volume fraction $\varphi_2 = \pi r_2^2(1 - \mathcal{R}_2^2)/b^2$ (resp. $\varphi_4 = \pi r_4^2(1 - \mathcal{R}_4^2)/b^2$). The porosity associated with the pore fluid network is $\phi_p = \varphi_2 + \varphi_4$.

For the sake of brevity in the presentation, semi-phenomenological models [27, 2, 14] will be used to cal-

Document downloaded by @DAEL, 2026-11-23 04:30:24 - personal use only

culate the dynamic permeabilities and pressure diffusion functions. The mathematical form of these models is

$$\mathcal{X}_\omega(\mathcal{X}_0, \varpi, \mathcal{M}) = \mathcal{X}_0 \left(\frac{\mathrm{j}\omega}{\varpi} + \sqrt{1 + \frac{\mathrm{j}\omega}{\varpi}\frac{\mathcal{M}}{2}} \right)^{-1}. \quad (37)$$

Here $\mathcal{X}_\omega$ is an effective parameter with $\mathcal{X}_0 = \mathcal{X}(\omega = 0)$ being its static value, ϖ is a characteristic frequency, and $\mathcal{M}$ is a shape factor (see e.g. [27, 2, 14]). What these represent will become apparent below.

To lighten the notation, the dependence on ω of the effective parameters will not be explicitly stated in the main text but only in the numbered equations from now on.

The dynamic viscous permeabilities of the annular pores and the granular material the local heterogeneities are made of are calculated as

$$\mathcal{K}_i(\omega) = \mathcal{X}_\omega \left(\mathcal{K}_{0i}, \frac{\eta\phi_i}{\rho_0 \mathcal{K}_{0i}\alpha_{\infty i}}, \frac{8\mathcal{K}_{0i}\alpha_{\infty i}}{\phi_i \Lambda_{vi}^2} \right). \quad (38)$$

These depend on physical parameters and geometrical ones, namely the porosities ϕ_i, static viscous permeabilities $\mathcal{K}_{0i}$, viscous characteristic lengths Λ_{vi}, and tortuosities $\alpha_{\infty i}$. The definitions of these parameters can be found in [1, 27] and their expressions for the material investigated here are summarised in Table I (see also the equations referred to in its caption and note that $\phi_i = \varphi_i$ for $i = 2, 4$; and $\phi_i = \phi_g$ and $r_i = r_g$ for $i = 1, 3, 5$). It is worth mentioning that for the local heterogeneities, $\mathcal{K}_i$ can be approximated by $\mathcal{K}_{0i}$ (for $i = 1, 3, 5$).

The dynamic thermal permeabilities Θ_i are calculated using Equation (39). Note that i) the expressions for the static thermal permeabilities Θ_{0i} and thermal characteristic lengths [28] Λ_{ti} required for their calculations are shown in Table I, and ii) Θ_i will be used to calculate C_p, C_i, and C (see Equations (27) and (28); and the latter equation with $p \to i$).

$$\Theta_i(\omega) = \mathcal{X}_\omega \left(\Theta_{0i}, \frac{\kappa\phi_i}{\rho_0 c_p \Theta_{0i}}, \frac{8\Theta_{0i}}{\phi_i \Lambda_{ti}^2} \right). \quad (39)$$

The pressure diffusion functions B_i (with $i = 1, 3, 5$) are calculated as

$$B_i(\omega) = \mathcal{X}_\omega \left(B_{0i}, \frac{\varphi_i \mathcal{D}_i(\omega)}{B_{0i}}, \frac{8B_{0i}}{\varphi_i \Lambda_{bi}^2} \right). \quad (40)$$

The parameters involved are the static values B_{0i} of the pressure diffusion functions, pressure diffusion characteristic lengths $\Lambda_{bi} = 2\Omega_i/\Gamma_i$, volume fractions φ_i, and pressure diffusivities $\mathcal{D}_i = \mathcal{K}_i/\eta\mathsf{C}_i$. The expressions for B_{0i} and Λ_{bi} are shown in Table II.

The effective parameters associated with the pore fluid network are calculated using a parallel flow model [14], i.e. $\mathcal{K}_p = \mathcal{K}_2 + \mathcal{K}_4$ and $\mathsf{C}_p = \mathsf{C}_2 + \mathsf{C}_4$. The dynamic viscous permeability and effective compressibility of the material are then calculated as $\mathcal{K} = \mathcal{K}_p$ and $\mathsf{C} = \mathsf{C}_p + \sum_{i=1,3,5} \varphi_i \mathsf{C}_i \mathcal{F}_i$, with $\mathcal{F}_i$ being calculated using Equation (30) and C_i by Equation (28) (with $p \to i$). Let us remind

Table I. Parameters of the model for the dynamic permeabilities of the substrate granular material composing the local heterogeneities $\Omega_{1,3,5}$ [31, 32] and the annular pores Ω_2 and Ω_4 [33]. See also Figure 2 and Equations (41)–(46).

	$\Omega_{i=1,3,5}$	$\Omega_{i=2,4}$
$\mathcal{K}_{0i}$	$\mathrm{K}(\sqrt[3]{1-\phi_g}, r_g)$	$\mathbb{K}(\varphi_i, r_i, r_{i-1}/r_i)$
Λ_{vi}	$\mathrm{L}_v(\phi_g, r_g)$	$\mathbb{L}(r_i, r_{i-1}/r_i)$
$\alpha_{\infty i}$	$\mathrm{A}_\infty(\phi_g)$	$\mathbb{A}_\infty$
Θ_{0i}	$\mathrm{T}(\sqrt[3]{1-\phi_g}, r_g)$	$\mathbb{K}(\varphi_i, r_i, r_{i-1}/r_i)$
Λ_{ti}	$\mathrm{L}_t(\phi_g, r_g)$	$\mathbb{L}(r_i, r_{i-1}/r_i)$

Table II. Parameters of the model for the pressure diffusion functions of the porous cylindrical inclusions Ω_1 [29], annular inclusions Ω_3, and matrix Ω_5 [14]. See also Figure 2 and Equations (45)–(48).

	$\Omega_{i=1}$	$\Omega_{i=3}$	$\Omega_{i=5}$
B_{0i}	$\mathbb{K}(\varphi_i, r_i, 0)$	$\mathbb{K}(\varphi_i, r_i, r_{i-1}/r_i)$	$\varsigma(\varphi_i, r_{i-1})$
Λ_{bi}	$\mathbb{L}(r_i, 0)$	$\mathbb{L}(r_i, r_{i-1}/r_i)$	$\mathcal{L}_t(\varphi_i, r_{i-1})$

that the latter may be approximated by their static value $\mathsf{C}_{0i} = \phi_i/P_0$ (with $i = 1, 3, 5$) and consequently $\mathcal{D}_i$ take the values $P_0\mathcal{K}_{0i}/\eta\phi_i$.

We recall that the formulas for the macroparameters quoted in Tables I and II, namely those for the static viscous and thermal permeabilities, tortuosities, viscous and thermal characteristic lengths, static values of the pressure diffusion function and pressure diffusion characteristic lengths are given by

$$\mathrm{K}(\beta, r) = \frac{r^2}{3\beta^2}\left(\frac{2+3\beta^5}{\beta(3+2\beta^5)} - 1 \right), \quad (41)$$

$$\mathrm{T}(\beta, r) = \frac{r^2}{15}\frac{5 - 9\beta + 5\beta^3 - \beta^6}{\beta^3}, \quad (42)$$

$$\mathrm{L}_v(\phi, r) = \frac{2}{9} r\phi \frac{(3-\phi)}{(1-\phi)}, \quad \mathrm{L}_t(\phi, r) = \frac{2}{3} r \frac{\phi}{1-\phi}, \quad (43)$$

$$\mathrm{A}_\infty(\phi) = \frac{3-\phi}{2}, \quad \mathbb{A}_\infty = 1, \quad \mathcal{A}_\infty(\phi) = 2 - \phi, \quad (44)$$

$$\mathbb{K}(\varphi, r, \mathcal{R}) = \varphi\frac{r^2}{8}\left(1 + \mathcal{R}^2 - \frac{1-\mathcal{R}^2}{\ln(1/\mathcal{R})} \right), \quad (45)$$

$$\mathbb{L}(r, \mathcal{R}) = r(1-\mathcal{R}), \quad (46)$$

$$\varsigma(\varphi, r) = \frac{r^2}{8}\frac{-2\ln(1-\varphi) - 2\varphi - \varphi^2}{(1-\varphi)}, \quad (47)$$

$$\mathcal{L}_t(\varphi, r) = r\frac{\varphi}{1-\varphi}, \quad \mathcal{L}_v(\varphi, r) = r\frac{\varphi(2-\varphi)}{2(1-\varphi)}. \quad (48)$$

3.2. Acoustical properties

The acoustical properties of an air-saturated perforated porous matrix with concentric annular and cylindrical porous inclusions co-axially inserted in the perforations (or heterogeneous sound absorber) are illustrated in this section. We consider the following geometrical parameters of the material (see Figure 2): $r_1 = 10\,\mathrm{mm}$, $r_2 = 12\,\mathrm{mm}$,

Document downloaded by @DAEL, 2026-11-23 04:30:24 - personal use only

$r_3 = 19.5$ mm, $r_4 = 21.5$ mm, and $b = 53$ mm. The volume fractions of the local heterogeneities are $\varphi_1 = 0.1118$, $\varphi_3 = 0.2642$, and $\varphi_5 = 0.4830$; while the mesoporosity is $\phi_p = \varphi_2 + \varphi_4 = 0.0492 + 0.0917 = 0.1409$. The porous matrix and inclusions are made of the same granular material having grain radius $r_g = 50$ μm and porosity $\phi_g = 0.3$. The total porosity of the material is $\Phi = 0.3986$. Normal pressure ($P_0 = 101325$ Pa) and temperature ($T_0 = 293.15$ K) conditions are considered.

Figure 3 shows the normalised effective compressibility of the heterogeneous sound absorber. This is compared with that of i) the granular material substrate, and ii) a material with perfectly impervious local heterogeneities (or a bi-dispersed array of annular pores). The effective compressibility of the heterogeneous sound absorber is largely determined by the pressure diffusion characteristic frequencies $f_{b5} = 362.5$ Hz, $f_{b1} = 806.3$ Hz, and $f_{b3} = 2141.8$ Hz.

At low frequencies, the real part of the effective compressibility tends to the value predicted by Equation (32). As the frequency increases, this quantity decreases and shows transitions determined by the characteristic frequencies, while at high frequencies the limiting value predicted by Equation (32) is reached. In comparison with a bi-dispersed array of annular pores (resp. the substrate granular material), the real part of the effective compressibility coincide at high frequencies, while this is increased by a factor of Φ/ϕ_p (resp. Φ/ϕ_m) at low frequencies. In the audible frequency range, and for this example, sound propagation in the most permeable fluid network (resp. substrate material) is quasi adiabatic (resp. quasi isothermal), as can be seen by comparing the grey and black dashed curves in Figure 3. Hence the attenuation of sound in the heterogeneous absorber is mainly caused by the pressure diffusion phenomena that occur in the geometrically-induced local heterogeneities. This is illustrated in Figure 3b where the acoustic losses in the material are shown to be largely determined by the characteristic frequencies associated with the pressure diffusion phenomena. Due to the preponderant role of these characteristic frequencies f_{bi}, they can be used for material design. For example, consider a substrate granular material with an associated pressure diffusivity of $\mathcal{D}_{0i} = 0.1$ m^2/s (with $i = 1, 3, 5$), which is a value obtained for $\phi_g = 0.3$ and $r_g \approx 62.8$ μm. One may want to have $\omega_{b1}/\omega_{b3} = 1/2$ and $\omega_{b1}/\omega_{b5} = 2$ with $f_{b1} = 1000$ Hz, i.e. $f_{b3} = 2000$ Hz and $f_{b5} = 500$ Hz.

From the expression for ω_{b1} (see Equation (31) and Table II), one can obtain the radius $r_1 = \sqrt{8\mathcal{D}_{01}/\omega_{b1}} \approx 11.3$ mm. Using the frequency ratio $\omega_{b1}/\omega_{b3} = (1 + \mathcal{R}_3^2 - (1 - \mathcal{R}_3^2)/\ln(1/\mathcal{R}_3))/\mathcal{R}_3^2\mathcal{R}_2^2$ one can select a value for $\mathcal{R}_3 = 0.7$ and obtain that of $\mathcal{R}_2 = 0.4954$. These can then be used to calculate $r_2 = r_1/\mathcal{R}_2 \approx 22.8$ mm and $r_3 = r_2/\mathcal{R}_3 \approx 32.5$ mm. Considering the frequency ratio $\omega_{b1}/\omega_{b5} = (-2\ln(1-\varphi_5) - 2\varphi_5 - \varphi_5^2)/\varphi_5(1-\varphi_5)\mathcal{R}_4^2\mathcal{R}_3^2\mathcal{R}_2^2$, one can select a value for $\varphi_5 = 0.3$ and obtain $\mathcal{R}_4 = 0.6799$, i.e. $r_4 \approx 47.9$ mm, which leads to a cell size $b \approx 101.4$ mm.

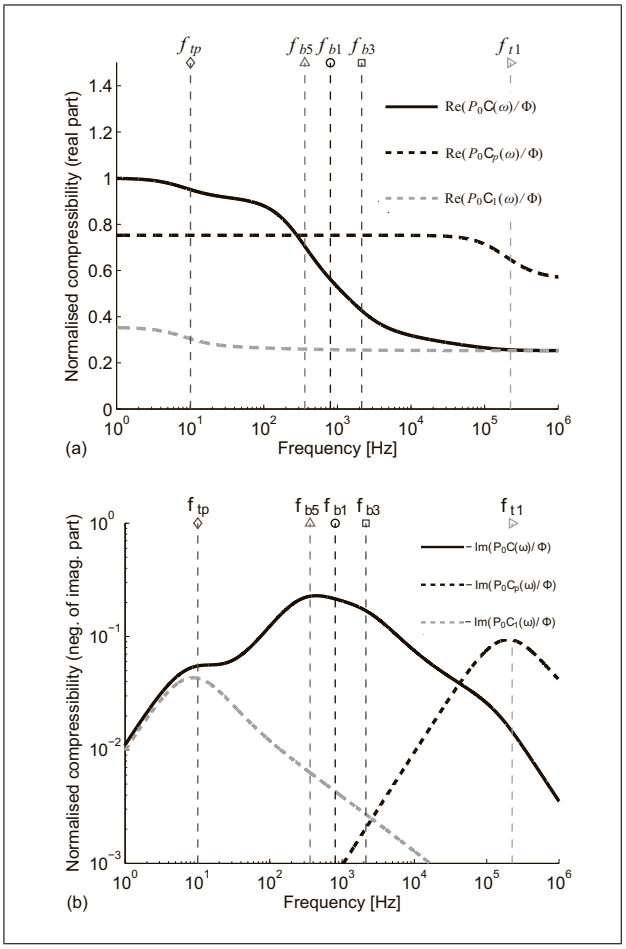

Figure 3. Normalised effective compressibility as a function of frequency. (a) Real part. (b) Negative of the imaginary part. Continuous black line – Perforated porous matrix with concentric porous annular and cylindrical inclusions co-axially inserted in the perforations. Dashed black line – Bi-dispersed array of annular pores (i.e. perfectly impervious local heterogeneities). Dashed grey lines – Substrate granular material. The vertical lines with markers represent characteristic frequencies.

Figure 4 shows the normal incidence sound absorption coefficient of a rigidly-backed 5-cm thick layer of the heterogeneous sound absorber (a) in comparison with that of the granular material substrate (f), a bi-dispersed array of annular pores (e), a perforated porous matrix [14] (d), a perforated matrix with cylindrical porous inclusion inserted in the perforations [22] (c), and a perforated matrix with annular porous inclusions inserted in the perforations (b).

The circles represent finite element calculations obtained by solving the set of equations (1)–(7), i.e. a linearised oscillatory Stokes-Fourier problem formulated in the pore space interacting with the local heterogeneities modelled as Darcy media has been solved. A good agreement between the theoretical prediction and numerical results is obtained.

In this example, a comparison between the curves (a)–(c) and (d) shows that by inserting annular and cylindrical porous inclusions in the matrix perforations one can substantially improve the absorptive properties of the per-

Document downloaded by @DAEL, 2026-11-23 04:30:24 - personal use only

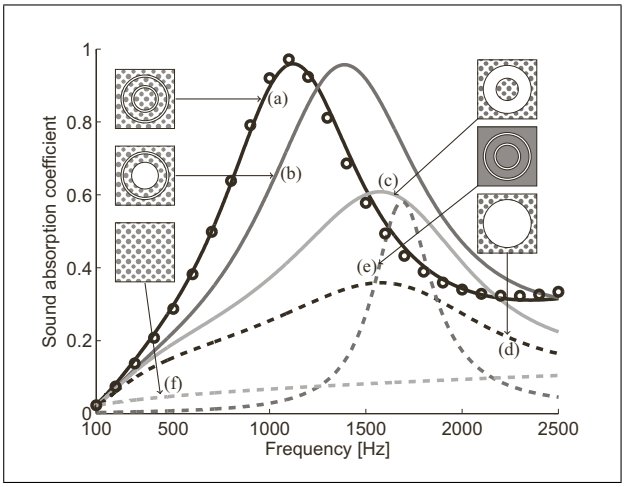

Figure 4. Sound absorption coefficient of rigidly-backed 5-cm thick material layers. (a) Perforated porous matrix (PPM) with concentric annular and cylindrical porous inclusions co-axially inserted in the perforations. (b) PPM with annular porous inclusion. (c) PPM with cylindrical porous inclusions. (d) PPM. (e) Perfectly impervious local heterogeneities (i.e. array of bi-dispersed annular pores). (f) Granular material substrate. The parameters are as in Figure 3 and the circles represent direct numerical calculations (see the text for more details).

forated matrix (or double porosity material). In addition, it is clear that by introducing geometrical heterogeneities a highly resistive granular layer can be transformed into a much more efficient sound absorber. On the other hand, the absorptive peak can be tuned at a much lower frequency than that of a material with perfectly impervious local heterogeneities.

4. Material with local material heterogeneities

The previous section exemplified the concept of introducing geometrical heterogeneities to induce local non-equilibrium pressure states in permeable heterogeneous materials with the aim of enhancing sound attenuation. In this section, instead, material heterogeneities are introduced for the same purpose.

An analytical model for the acoustical properties of a heterogeneous array of porous cylinders made of different substrate porous materials is first introduced and some examples of its acoustic behaviour follow.

4.1. Analytical model

Figure 5 shows the geometry and elementary cell of an array of porous cylinders made of different substrate porous materials, i.e. a heterogeneous array of porous cylinders. The elementary cell features local heterogeneities (or porous cylinders) Ω_1, Ω_2, and Ω_3; and a pore fluid network Ω_p. Sound propagation perpendicular to the cylinder axes is considered.

The porous cylinders Ω_i (with $i = 1, 2, 3$) have radius r_c and volume fractions $\varphi_i = (1 - \phi_p)/n$ with $n = 3$,

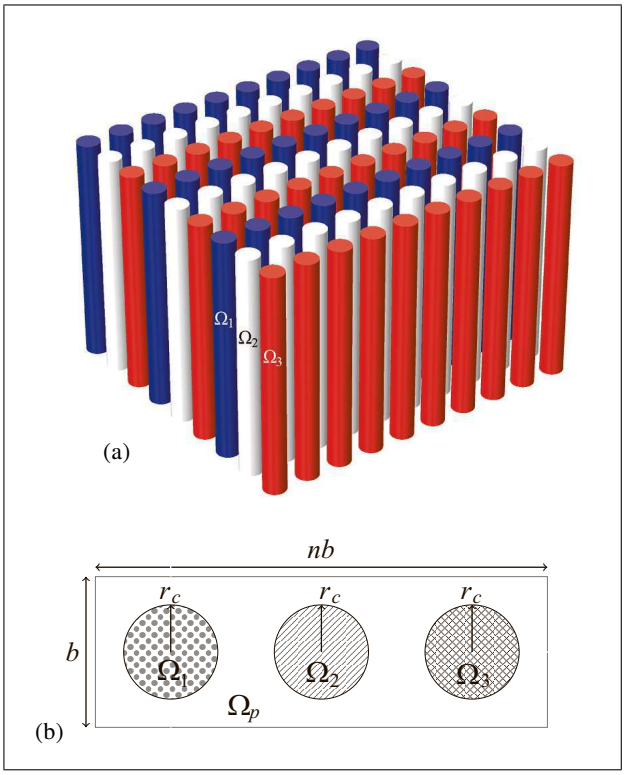

Figure 5. (Colour online) Geometry (a) and elementary cell (b) of an array of porous cylinders of radius r_c made of different substrate porous materials. The pore fluid network is represented by Ω_p and the local heterogeneities by Ω_i with $i = 1, 2, 3$. The cell size has dimensions b by nb with $n = 3$ and sound propagation is perpendicular to the cylinder axes.

and are made out of different substrate granular materials, being each one of them characterised by their grain radius r_i and porosity ϕ_i. The porosity of the pore fluid network is $\phi_p = 1 - \pi r_c^2/b^2 = \varphi_p$.

As previously, semi-phenomenological models [27, 2, 14] of the type shown in Equation (37) are used to calculate the dynamic permeabilities and pressure diffusion functions.

The dynamic viscous and thermal permeabilities of the substrate granular materials, $\mathcal{K}_i$ and Θ_i (with $i = 1, 2, 3$), are given by Equations (38) and (39), and are calculated using the parameters shown in Table III. Note that $\mathcal{K}_i$ can be approximated by $\mathcal{K}_{0i}$. The pressure diffusion functions B_i are given by Equation (40) with $\mathcal{D}_i = \mathcal{K}_i/\eta \mathsf{C}_i$ and the parameters [29] used for their calculation are also shown in Table III. Let us recall that $\mathbb{K}(\varphi, r, \mathcal{R} = 0) = \varphi r^2/8$ and $\mathbb{L}(r, \mathcal{R} = 0) = r$.

The permeabilities associated with the pore fluid network, $\mathcal{K}_p = \mathcal{K}_{i=p}$ and $\Theta_p = \Theta_{i=p}$, are also given by Equations (38) and (39) and are calculated using the parameters [30] shown in Table III.

The dynamic viscous permeability and effective compressibility of the heterogeneous array of porous cylinders are then calculated as $\mathcal{K} = \mathcal{K}_p$ and $\mathsf{C} = \mathsf{C}_p + \sum_{i=1,2,3} \varphi_i \mathsf{C}_i \mathcal{F}_i$, with C_i and $\mathcal{F}_i$ being calculated using Equations (28) (with $p \to i$) and (30). We recall that C_i may be approximated by ϕ_i/P_0 (with $i = 1, 2, 3$).

Document downloaded by @DAEL, 2026-11-23 04:30:24 - personal use only

Table III. Parameters of the model for the dynamic permeabilities and pressure diffusion functions of a heterogeneous array of porous cylinders. See also Figure 5 and Equations (41)–(48).

	$\Omega_{i=p}$	$\Omega_{i=1,2,3}$
$\mathcal{K}_{0i}$	$\varsigma(\phi_p, r_c)/2$	$\mathrm{K}(\sqrt[3]{1-\phi_i}, r_i)$
Λ_{vi}	$\mathcal{L}_v(\phi_p, r_c)$	$\mathrm{L}_v(\phi_i, r_i)$
$\alpha_{\infty i}$	$\mathcal{A}_\infty(\phi_p)$	$\mathrm{A}_\infty(\phi_i)$
Θ_{0i}	$\varsigma(\phi_p, r_c)$	$\mathrm{T}(\sqrt[3]{1-\phi_i}, r_i)$
Λ_{ti}	$\mathcal{L}_t(\phi_p, r_c)$	$\mathrm{L}_t(\phi_i, r_i)$
$\boldsymbol{B}_{0i}$	—	$\mathbb{K}(\varphi_i, r_i, 0)$
Λ_{bi}	—	$\mathbb{L}(r_i, 0)$

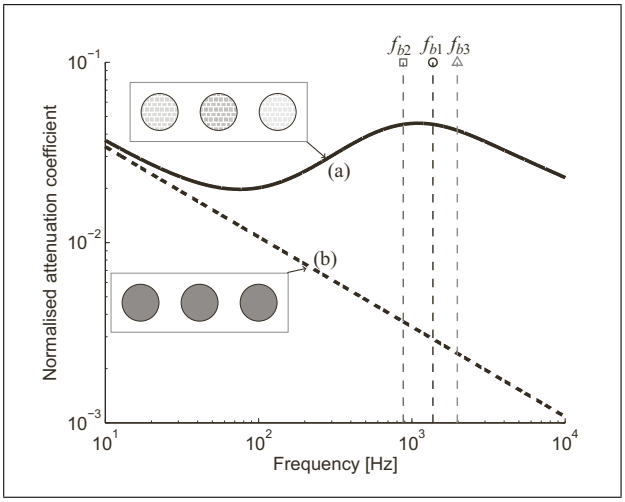

Figure 6. Normalised attenuation coefficient $-\mathrm{Im}(k_c(\omega)c_0/\omega)$ of a heterogeneous array of porous cylinders (a) and an array of impervious cylinders (b). The vertical lines with markers represent characteristic frequencies.

4.2. Acoustical properties

Figure 6 shows the normalised attenuation coefficient of a heterogeneous array of porous cylinders in comparison with that of a material with perfectly impervious cylinders. The parameters of the material are $r_c = 10\,\mathrm{mm}$, $\phi_p = 0.7$, $r_1 = 50\ \mu\mathrm{m}$, $r_2 = 0.8r_1$, $r_3 = 1.2r_1$, $\phi_1 = \phi_2 = \phi_3 = 0.36$, and $b = r_c\sqrt{\pi/(1-\phi_p)} \approx 32.36\,\mathrm{mm}$. It is clear that the heterogeneous array of porous cylinders attenuate sound more efficiently than an array of impervious cylinders, particularly around the characteristic frequencies f_{bi}.

Figure 7 shows the normal incidence sound absorption coefficient of a rigidly-backed layer of a heterogeneous array of porous cylinders in comparison with that of i) the different substrate granular materials, and ii) a material with perfectly impervious cylinders. The material parameters are as in Figure 6 and the layer thickness is $d = 10b$. The plot shows that the analytical model correctly captures the physics and its prediction compares well with the numerical simulation. Furthermore, the heterogeneous array provides much higher sound absorption coefficient values than i) any of the substrate materials having the same thickness d and ii) an array of impervious cylinders with the same cylinder radius r_c, mesoporosity ϕ_p, and layer

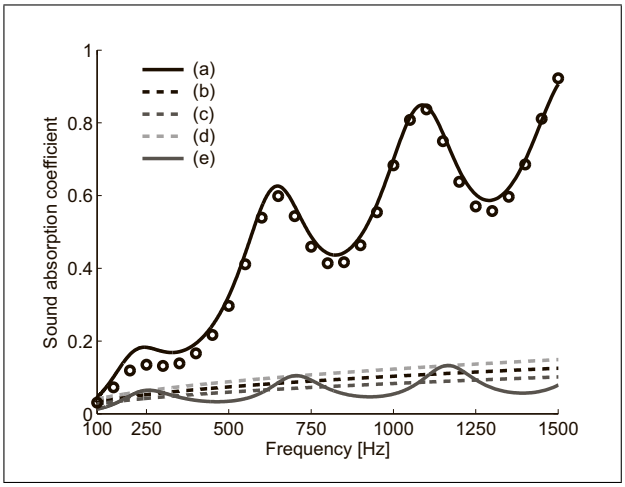

Figure 7. Normal incidence sound absorption coefficient of rigidly-backed layer of a heterogeneous array of porous cylinders (a), substrate material of Ω_1 (b), Ω_2 (c), and Ω_3 (d); and an array of impervious cylinders (e). The circles represent full wave numerical calculations.

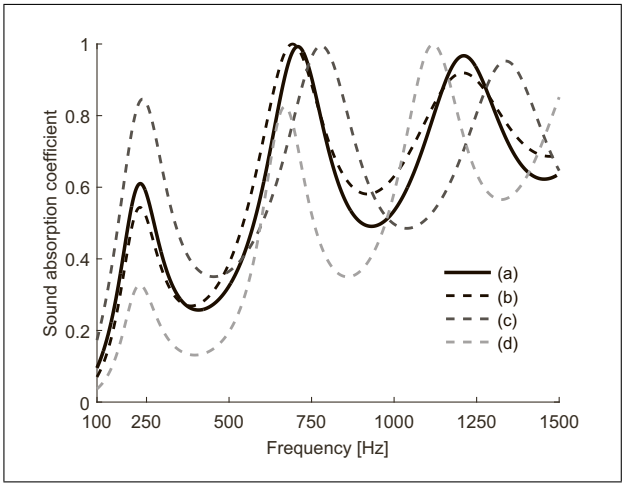

Figure 8. Normal incident sound absorption coefficient of rigidly-backed material layer of a heterogeneous array of porous cylinders (a) and double porosity array of porous cylinders made of a single substrate porous material Ω_1 (b), Ω_2 (c), and Ω_3 (d). See the main text for more details.

thickness d. This provides a useful way of utilising different highly resistive porous materials to design and build efficient sound absorbers.

Figure 8 shows the sound absorption coefficient of a rigidly-backed layer of a heterogeneous array of porous cylinders with parameters $\phi_p = 0.4$, $r_c = 10\,\mathrm{mm}$, $r_1 = 50\ \mu\mathrm{m}$, $r_2 = 0.5r_1$, $r_3 = 2r_1$, $\phi_1 = \phi_2 = \phi_3 = 0.36$, and $d = 10b \approx 22.8\,\mathrm{cm}$.

This is compared with that of different arrays of porous cylinders made of the same substrate material (or double porosity fibrous materials [29]). For example, the curve (b) represents the normal incidence sound absorption coefficient of an array of porous cylinders made of a substrate granular material having parameters r_1 and ϕ_1. In comparison with the sound absorption of the heterogeneous array

Document downloaded by @DAEL, 2026-11-23 04:30:24 - personal use only

with larger mesoporosity shown in Figure 7, the one presented in Figure 8 shows higher sound absorption coefficient values. This is because the contribution of the local heterogeneities to the overall sound energy dissipation is larger as their volume fraction increases (see the factor φ_i in Equation (27)).

This plot also shows that the sound absorption coefficient of the heterogeneous array, featuring three pressure diffusion characteristic frequencies $f_{b1} = 1374\,\text{Hz}$, $f_{b2} = 344\,\text{Hz}$, $f_{b3} = 5479\,\text{Hz}$, is similar to that of a double porosity array made of a single substrate material with its unique pressure diffusion characteristic frequency having a value close to the one that has the intermediate value in the heterogeneous array, i.e. to f_{b1} in this example.

5. Conclusions

Sound propagation in permeable heterogeneous materials has been investigated in this paper. These materials are characterised by a highly permeable pore fluid network and multiple much less permeable local heterogeneities. Their distinctive feature is that non-equilibrium pressure states of diffusive type occur locally. The key requisite for these states to exist is that the mass flux pulsed from the local heterogeneities on their common interface with the pores of the highly permeable pore fluid network is of one order smaller than the mass flux generated by the carrying wave in the pores. Being this requisite fulfilled, i) the fluid flow, at the leading order, is mainly determined by that in the pores, which means that the dynamic viscous permeability of the material is well approximated by that of the highly permeable pore fluid network; and ii) the influence of the local non-equilibrium pressures states on the acoustical properties of the material are accounted for by a modified effective compressibility. Such a modification leads to enhanced dissipation of sound energy around the multiple tunable characteristic frequencies associated with the local phenomena.

To put forward the concept of inducing local non-equilibrium pressure states in permeable heterogeneous materials by means of introducing geometrical or material heterogeneities and illustrate the acoustic behaviour of the investigated class of materials, we have introduced analytical models for the long-wavelength acoustical properties of i) a perforated porous matrix with concentric annular and cylindrical porous inclusions co-axially inserted in the perforations (see Figure 2), and ii) a heterogeneous array of highly resistive porous cylinders (see Figure 5). The model predictions have been compared with numerical simulations showing good agreement.

This allowed us to conclude that introducing either local geometrical or material heterogeneities has a strong influence on the acoustical properties of the material. In particular, the sound attenuation is largely increased around the characteristic frequencies associated with the local non-equilibrium pressure states. Furthermore, we have demonstrated that the investigated class of materials can provide much improved sound attenuation than conventional highly resistive porous materials. This opens up new possibilities for the design of acoustic materials with enhanced sound attenuation caused by pressure diffusion, which can be interpreted as a non-conventional manifestation of the mechanisms of sound energy dissipation associated with viscosity and heat transfer effects.

Acknowledgements

This work has been supported by the project METAUDIBLE, co-funded by the Agence Nationale de la Recherche ANR (ANR 13-BS09-0003-03) and Fondation de Recherche pour l'Aéronautique et l'Espace FRAE, and was conducted within the framework of CeLyA of Université de Lyon operated by ANR (ANR 10 Labex 0060 and ANR 11 IDEX - 0007). This work has also been supported by Conicyt-Fondecyt under Research Grant Number 1171110. Dissemination of this work was supported by COST (European Cooperation in Science and Technology) through the COST Action CA15125 "Designs for Noise Reducing Materials and Structures" (DENORMS).

Appendix

This appendix presents the leading-order problems determining the non-equilibrium pressure states in the local heterogeneities.

Identifying terms of like-power in Equations (20) and (21), one obtains at ε^0 that the leading-order pressures $p_i^{*(0)}$ in the local heterogeneities are governed by Equations (A1) with the macroscopic pressure $p^{*(0)}$ acting as a forcing term on the interfaces Γ_i^*, as shown by Equation(A2); namely

$$\mathbb{D}_{ic}\nabla_{\mathbf{y}^*}\cdot(\mathcal{D}_i^*\nabla_{\mathbf{y}^*}p_i^{*(0)}) = \mathrm{j}\omega^* p_i^{*(0)} \quad \text{in} \quad \Omega_i^*, \qquad \text{(A1)}$$

$$\mathbb{P}_{ic}p_i^{*(0)} = p^{*(0)} \quad \text{on} \quad \Gamma_i^*, \qquad \text{(A2)}$$

where the complex-valued frequency-dependent dimensionless pressure diffusivities $\mathcal{D}_i^*$ are given by

$$\mathcal{D}_i^*(\omega^*) = \frac{\mathcal{K}_i^*(\omega^*)}{\eta^*\mathsf{C}_i^*(\omega^*)}. \qquad \text{(A3)}$$

Note that, for simplicity in the notation, we have considered that the microporous materials are isotropic, i.e. $\mathbf{k}_i^* = \mathcal{K}_i^*\mathbf{I}$.

Inserting the auxiliary variables $\mathsf{P}_i^* = \mathbb{P}_{ic}p_i^{*(0)} - p^{*(0)}$ into Equations (A1)–(A2), one obtains the linear diffusion problems in dimensionless form,

$$\mathbb{D}_{ic}\nabla_{\mathbf{y}^*}\cdot\left(\mathcal{D}_i^*(\omega^*)\nabla_{\mathbf{y}^*}\mathsf{P}_i^*\right) = \mathrm{j}\omega^*\mathsf{P}_i^* + \mathrm{j}\omega^* p^{*(0)} \quad \text{in} \quad \Omega_i^*, \qquad \text{(A4)}$$

$$\mathsf{P}_i^* = 0 \quad \text{on} \quad \Gamma_i^*. \qquad \text{(A5)}$$

The unknown P_i^* can then be linearly related to $p^{*(0)}$ via [13, 14, 20]

$$\mathsf{P}_i^* = -\frac{b_i^*(\mathbf{y}^*,\omega^*)}{\mathbb{D}_{ic}\mathcal{D}_i^*(\omega^*)}\mathrm{j}\omega^* p^{*(0)}, \qquad \text{(A6)}$$

Document downloaded by @DAEL, 2026-11-23 04:30:24 - personal use only

where b_i^* represent the unknown Ω_p^* − periodic dimensionless local diffusive pressure fields normalised by $-\mathrm{j}\omega^* p^{*(0)}/\mathbb{D}_{ic}\mathcal{D}_i^*$.

Using the original variables, Equation (A6) can be rewritten as

$$\mathbb{P}_{ic} p_i^{*(0)} = p^{*(0)} \left(1 - \frac{\mathrm{j}\omega^* b_i^*(\mathbf{y}^*, \omega^*)}{\mathbb{D}_{ic}\mathcal{D}_i^*(\omega^*)}\right). \tag{A7}$$

Integrating this expression over the volume of the local heterogeneities and dividing by Ω^*, one obtains

$$\frac{1}{\Omega^*}\int_{\Omega_i^*} \mathbb{P}_{ic} p_i^{*(0)} \mathrm{d}\Omega^* = \varphi_i p^{*(0)} \left(1 - \frac{\mathrm{j}\omega^* B_i^*(\omega^*)}{\varphi_i \mathbb{D}_{ic}\mathcal{D}_i^*(\omega^*)}\right), \tag{A8}$$

where the dimensionless pressure diffusion functions B_i^* are given by

$$B_i^*(\omega^*) = \frac{1}{\Omega^*}\int_{\Omega_i^*} b_i^*(\mathbf{y}^*, \omega^*)\,\mathrm{d}\Omega^*. \tag{A9}$$

Let us finally write Equation (A8) in dimensional physical form. To do so, we recall that, for example, $p_i^{*(0)} = p_i^{(0)}/p_{ic}$, $p^{*(0)} = p^{(0)}/p_{pc}$, and so on.

Introducing these expressions into Equation (A8) and recalling that $\mathbb{P}_{ic} = p_{ic}/p_{pc}$ and $\mathbb{D}_{ic} = k_{ic}/\varrho^2\omega_c C_{ic}\eta_c$, one obtains

$$\frac{1}{\Omega}\int_{\Omega_i} p_i^{(0)} \mathrm{d}\Omega = \varphi_i p^{(0)} \left(1 - \frac{\mathrm{j}\omega B_i(\omega)}{\varphi_i \mathcal{D}_i(\omega)}\right), \tag{A10}$$

where the pressure diffusivities $\mathcal{D}_i$ and pressure diffusion functions B_i are given by

$$\mathcal{D}_i(\omega) = \frac{\mathcal{K}_i}{\eta \mathsf{C}_i}, \quad B_i(\omega) = \varrho^2 B_i^*. \tag{A11}$$

As introduced in [14], $B_i(\omega)$ can be calculated using a model of the type shown in Equation (37) [see also, for example, Equation (40)].

References

[1] J. L. Auriault, L. Borne, R. Chambon: Dynamics of porous saturated media, checking of the generalized law of Darcy. J. Acoust. Soc. Am. **77**(5) (1985) 1641–1650.

[2] D. Lafarge, P. Lemarinier, J. F. Allard, V. Tarnow: Dynamic compressibility of air in porous structures at audible frequencies. J. Acoust. Soc. Am. **102**(4) (1997) 1995–2006.

[3] J. L. Auriault, C. Boutin, C. Geindreau: Homogenization of Coupled Phenomena in Heterogeneous Media, ISTE Ltd and John Wiley & Sons, London and Hoboken, 2009.

[4] J. F. Allard, N. Atalla: Propagation of Sound in Porous Media: Modeling Sound Absorbing Materials, John Wiley & Sons, West Sussex, 2009.

[5] C. Boutin: Acoustics of porous media with inner resonators. J. Acoust. Soc. Am. **134**(6) (2013) 4717–4729.

[6] D. Lafarge, N. Nemati: Nonlocal Maxwellian theory of sound propagation in fluid-saturated rigid-framed porous media. Wave Motion **50**(6) (2013) 1016–1035.

[7] C. Lagarrigue, J.-P. Groby, V. Tournat, O. Dazel, O. Umnova: Absorption of sound by porous layers with embedded periodic array of resonant inclusions. J. Acoust. Soc. Am. **134** (2013) 4670–4680.

[8] C. Boutin, F. X. Becot: Theory and experiments on poro-acoustics with inner resonators. Wave Motion **54** (2015) 76–99.

[9] N. Nemati, A. Kumar, D. Lafarge, N. X. Fang: Nonlocal description of sound propagation through an array of Helmholtz resonators. CR Mécanique **343**(12) (2015) 656–669.

[10] J. P. Groby, A. Lardeau, W. Huang, Y. Auregan: The use of slow sound to design simple sound absorbing materials. J. Appl. Phys. **117** (2015) 124903.

[11] A. S. Elliott, R. Venegas, J.P. Groby, O. Umnova: Omnidirectional acoustic absorber with a porous core and a graded index matching layer. J. Appl. Phys. **115** (2014) 204902.

[12] T. Dupont, P. Leclaire,O. Sicot, X. L. Gong, R. Panneton: Acoustic properties of air-saturated porous materials containing dead-end porosity. J. Appl. Phys. **110**(9) (2011) 094903.

[13] C. Boutin, P. Royer, J. L. Auriault: Acoustic absorption of porous surfacing with dual porosity. Int. J. Solids Struct. **35** (1998) 4709–4737.

[14] X. Olny, C. Boutin: Acoustic wave propagation in double porosity media. J. Acoust. Soc. Am. **113**(6) (2003) 73–89.

[15] N. Atalla, F. Sgard, X. Olny, R. Panneton: Acoustic absorption of macro-perforated porous materials. J. Sound Vib. **243**(4) (2001) 659–678.

[16] F. Sgard, F. Castel, N. Atalla: Use of a hybrid adaptive finite element/modal approach to assess the sound absorption of porous materials with meso-heterogeneities. Appl. Acoust. **72** (2011) 157–168.

[17] R. Venegas, O. Umnova: Acoustical properties of double porosity granular materials. J. Acoust. Soc. Am. **130**(5) (2011) 2765–2776.

[18] R. Venegas, O. Umnova: Influence of sorption on sound propagation in granular activated carbon. J. Acoust. Soc. Am. **140**(2) (2016) 755–766.

[19] C. Boutin, R. Venegas: Assessment of the effective parameters of dual porosity deformable media. Mech. Mater. **102** (2016) 26–46.

[20] R. Venegas, C. Boutin: Acoustics of sorptive porous materials. Wave Motion **68** (2017) 162–181.

[21] R. Venegas, C. Boutin, O. Umnova: Acoustics of multiscale sorptive porous materials. Phys. Fluids **29** (2017) 082006.

[22] R. Venegas, C. Boutin: Acoustics of permeable heterogeneous materials with local non-equilibrium pressure states. J. Sound Vib. **418** (2018) 221–239.

[23] E. Gourdon, M. Seppi: Extension of double porosity model to porous materials containing specific porous inclusions. Acta Acust united Ac. **96** (2010) 275–291.

[24] F. Chevillotte, L. Jaouen, F.-X. Bécot: On the modeling of visco-thermal dissipations in heterogeneous porous media. J. Acoust. Soc. Am. **138**(6) (2015) 3922–3929.

[25] R. Venegas, C. Boutin: Acoustics of permeo-elastic materials, J. Fluid Mech. **828** (2017) 135–174.

[26] J.-L. Auriault: Heterogeneous medium. Is an equivalent macroscopic description possible? Int. J. Eng. Sci. **29** (7) (1991) 785–795.

[27] D. L. Johnson, J. Koplik, R. Dashen: Theory of dynamic permeability and tortuosity in fluid-saturated porous media. J. Fluid Mech. **176** (1987) 379–402.

Document downloaded by @DAEL, 2026-11-23 04:30:24 - personal use only

[28] Y. Champoux, J. F. Allard: Dynamic tortuosity and bulk modulus in air-saturated porous media. J. Appl. Phys. **70**(4) (1991) 1975–1979.

[29] R. Venegas: Microstructure influence on acoustical properties of multiscale porous materials, Ph.D. thesis, University of Salford, UK, 2011.

[30] O. Umnova, D. Tsiklauri, R. Venegas: Effect of boundary slip on the acoustical properties of microfibrous materials. J. Acoust. Soc. Am. **126**(4) (2009) 1850–1861.

[31] C. Boutin, C. Geindreau: Estimates and bounds of dynamic permeability of granular media. J. Acoust. Soc. Am. **124**(6), (2008) 3402–3411 (2008).

[32] C. Boutin, C. Geindreau: Periodic homogenization and consistent estimates of transport parameters through sphere and polyhedron packings in the whole porosity range. Phys. Rev. E **82** (2010) 036313.

[33] M. Nori, R. Venegas: Sound propagation in porous materials with annular pores, J. Acoust. Soc. Am. 141 (6) (2017) 4642–4651.

Document downloaded by @DAEL, 2026-11-23 04:30:24 - personal use only